Vol. 95: 141–154, 1993 | MARINE ECOLOGY PROGRESS SERIES
Mar. Ecol. Prog. Ser. | Published May 19

Photosynthesis-irradiance relationships and production associated with a warm-core ring shed from the Agulhas Retroflection south of Africa

K. M. Dower, M. I. Lucas

Southern Ocean Group, Marine Biology Research Institute, Department of Zoology, University of Cape Town, Private Bag, Rondebosch 7700, South Africa

ABSTRACT: Synoptic estimates of phytoplankton biomass and production in the world's oceans are dependent upon ocean colour remote sensing and suitable algorithms developed from simultaneous measurements of photosynthetic parameters and optical properties in the water column. This study presents Photosynthesis-Irradiance (P-I) parameters estimated for a warm-core ring shed from the Agulhas Retroflection, in autumn, in the region of the Sub-Tropical Convergence south of Africa. Comparisons are made between values within the ring, at its edge and outside the ring in surrounding Sub-Antarctic Water. The 1 % light depth within the warm-core ring ranged from 38 to 92 m, 40 to 54 m at the edge and 40 to 75 m outside the ring. Chlorophyll *a* (chl *a*) concentrations in surface waters increased from ca 0.43 mg m^{-3} within the ring to about 1.0 mg m^{-3} at the ring edge and outside the ring. Size-fractionated chl *a* demonstrated that >56 % of the phytoplankton were <20 µm in size within the warm-core ring while outside the ring this figure was about 30 %. Picoplankton <3 µm made up between 8 and 9 % of the biomass at all sites. Considerable variability in photosynthetic parameters was found at all stations. Overall, the mean surface P^B_{max} (max. production rate) and α^B (initial slope of P-I curve) were 1.59 ± 0.13 mg C (mg chl *a*)$^{-1}$ h^{-1} and 0.046 ± 0.01 mg C (mg chl *a*)$^{-1}$ h^{-1} (µE m^{-2} s^{-1})$^{-1}$ Throughout, α^B was higher at 100 m and I_k (irradiance of saturation) lower. Production integrated to 100 m was lowest inside the ring (287 mg C m^{-2} d^{-1}), intermediate outside (404 mg C m^{-2} d^{-1}) and highest at the ring edge (453 mg C m^{-2} d^{-1}). We argue that production within the warm-core ring is limited by convective instability while outside the ring photosynthesis is probably limited by light, since nutrients are non-limiting. The edge of the ring exhibits highest production because of stability conferred by the warm-core ring water and a more favourable light environment. In terms of defining 'bio-optical provinces' based on remote sensing and photosynthetic parameters, we have identified a hydrographic area south of Africa covering the Sub-Tropical Convergence (STC) where there are reliable Coastal Zone Colour Scanner data which provide an average annual chl *a* concentration estimate of 0.49 mg m^{-3}. For this area we estimate total production integrated to 100 m to range from 10.5×10^2 to 16.5×10^2 t C km^{-2} yr^{-1}, ca 0.5 to 0.8 % of the global oceanic production. This confirms the importance of the STC as a potential biogenic sink for atmospheric CO_2.

INTRODUCTION

The global monitoring of oceanic phytoplankton production to estimate photosynthetic 'draw-down' of atmospheric CO_2 using satellite imagery with ocean colour sensors and well-developed algorithms has recently received much consideration (Platt et al. 1988, Morel & Berthon 1989, Mueller & Lange 1989, Sathyendranath et al. 1989, Kuring et al. 1990). Satellites are being increasingly used to overcome the restraints on ship-based sampling of highly variable oceanographic features (Kuring et al. 1990). A collage of regional chlorophyll 'maps' of the surface layer of the water column and sea-surface irradiance information have previously been derived from the NOAA NIMBUS 7 Coastal Zone Colour Scanner (CZCS) data (1978–1986) and transformed into production 'maps' of the euphotic layer using ship-based data, although coverage was incomplete. Future remote sensing of ocean colour by, amongst others, the sea-viewing wide-field-

of-view sensor (Sea WiFS), to be launched by NASA on the SeaStar mission in August 1993, will provide improved chl *a* concentration estimates with improved corrections for atmospheric aerosols and non-chlorophyll reflecting particles in the water column. Nevertheless, reliable and extensive 'ground truthing' of vertical pigment profiles, photosynthetic parameters and optical properties of the water column are required to accurately estimate water column production based on region-specific algorithms (Sathyendranath et al. 1989). These observations will assist international climate change programmes (e.g. Joint Global Ocean Flux Study) to divide the world oceans into 'bio-optical provinces' and provide one of many approaches in the estimation of basin-scale primary production.

The relationship between phytoplankton production and irradiance is central to the understanding of phytoplankton ecology and physiology and has for many years been used to estimate primary production in the ocean. Parameters derived from this relationship include P^B_{max}, a measure of photosynthetic capacity, and α^B, the initial slope of the P-I curve and a measure of the quantum efficiency of photosynthesis. In many cases photoinhibition is evident at high light intensities; this can be quantified by the parameter, β, the negative slope of the decline in photosynthesis beyond the optimal light intensity. Two additional light-dependent parameters can be derived from the above: I_k ($= P^B_{max}/\alpha^B$), the light intensity at the onset of photosynthetic saturation which may also be referred to as the index of photoadaptation and is a good indicator of photosynthetic efficiency at low light levels; and I_b, the light intensity where photoinhibition first becomes apparent.

Photosynthesis-irradiance curves therefore provide essential information defining spatial and temporal variability in light-dependent phytoplankton production by means of the described parameters. Variations in the parameters can be explained by environmental or growth conditions, depth, region and season and ultimately lead to a better understanding of algal physiology and water column production. With respect to *in situ* rates of primary production, the data derived from P-I curves are used effectively in, and contribute invaluable data towards, the setting up and development of algorithms essential to the remote sensing of integrated water column production.

The Southern Ocean south of Africa in the region of the Sub-Tropical Convergence (STC) is considered to be a particularly significant sink for atmospheric CO_2 due to elevated chl *a* concentrations, particularly on the northern edge of this front (Plancke 1977) and because of surface water subduction associated with South Atlantic Central Water formation (Lutjeharms et al. 1985). Chlorophyll concentrations in the frontal region have been recorded up to 1.7 mg m^{-3} (Boden 1988) compared to values of <0.5 mg m^{-3} for the surrounding water (El Sayed et al. 1979, Allanson et al. 1981, Boden 1988, Perissinotto et al. 1992). Satellite imagery colour composites show that the STC exhibits a strong seasonal and inter-annual signal that extends from South Africa almost to Australia with the greatest activity associated with the Agulhas Retroflection boundary where thermal gradients are strongest (Weeks & Shillington unpubl.). However, this region and the Southern Ocean in general, recognised to be important by JGOFS in terms of CO_2 flux and climate change, is characterized by a paucity of data concerned with remote sensing and biogenic CO_2 drawdown.

Eddies and warm-core rings are regularly shed from the Agulhas Retroflection in the region of the STC. An average of 9 rings are formed annually, some lasting as long as 2 years (Lutjeharms 1989, Duncombe Rae 1991, Gordon et al. 1992). Movement is generally towards the southeast Atlantic (Gordon 1985, Lutjeharms & Valentine 1988) which contributes to the control of the temperature and salt flux between the Indian and Atlantic oceans as Indian Ocean water enters the South Atlantic at a rate of between 3 and 20 × 10^6 m^3 s^{-1} (Duncombe Rae 1991, Gordon et al. 1992). The STC itself is a well-defined but highly variable feature due to latitudinal movements of the front and frequent eddy shedding (Lutjeharms 1989). It is also often characterised by high primary productivity (up to 88 mg C m^{-2} h^{-1}; Boden 1988) on its northern edge due most likely to improved vertical stability and mixing of nutrient rich Sub-Antarctic Surface Water into the nutrient impoverished Agulhas Current Waters (Allanson et al. 1981, Lutjeharms et al. 1985).

On a voyage of the MV 'SA Agulhas' to Marion Island (Prince Edward Islands, 46° 54' S, 37° 45' E) in April 1991 (austral autumn) a warm-core ring was identified and studied with the objective of estimating primary production, heat and CO_2 flux. Here we report on the measurement of photosynthesis-irradiance parameters and the calculation of daily water column production which will provide much needed ship-based data to be linked to future remote sensing and regional algorithm development.

METHODS

Study area and hydrography. A total of 37 stations were sampled along transects through the warm-core ring shed from the Agulhas Retroflection in the region of the Sub-Tropical Convergence zone, 42° 30' S, 22° 40' E (Fig. 1). Temperature profiles to

800 m were obtained using expandable bathythermographs (XBTs) and a conductivity temperature depth probe (CDT) was deployed to 500 m to determine the temperature-salinity structure. Water samples were collected in 8 l Niskin bottles for chl *a* and nutrient profiles. Thirteen stations were used as 'production stations' where light attenuation curves were calculated using a Biospherical Instruments 4π spherical underwater scalar irradiance sensor (QSP-200D) and a solar hemispherical sensor (QSP-240) for on-deck referencing. Surface (100 % light) and 100 m (<0.1 % light) water samples were used to estimate photosynthetic parameters. All water samples were kept in the dark until processed. Surface water samples were incubated immediately and the deep samples were processed after the first incubation, within 2 h. Of the 13 daily production stations, 6 were three 48 h stations with 2 day-time data pairs each. Although the data pairs were collected at the same coordinates, they were not necessarily from the same water as the hydrographic system is particularly dynamic. The sample pairs have therefore been treated as 2 separate stations. All production stations were undertaken at approximately 08:00 h local time. For the first 2 production stations (88 & 105) the deep sample was taken at 40 and 44 m respectively (the 1 % light depths) instead of sampling at 100 m. The thermocline at Stn 88 occurred at 20 m; above the 1 % light depth. The deep sample of this station was therefore included with the other 100 m samples. At Stn 105 the thermocline was below the 1 % light depth and so, for consistency, the deep sample of this station was excluded from the data.

After using the XBT data to determine the 10 °C isotherm around and within the ring, we subjectively divided the stations into those occurring where the 10 °C isotherm was shallower than 250 m depth (outside the ring), those where the 10 °C isotherm was between 250 and 500 m (ring edge) and those where the 10 °C isotherm exceeded 500 m (inside the ring). This gave 14 stations outside (5 production), 11 stations inside (4 production) and 12 stations at the ring edge (4 production).

Chlorophyll and primary production. After filtration of between 500 and 1000 ml seawater through <200 and <20 µm Nitex plankton screens and through <3 µm Nuclepore filters, the samples were finally filtered onto Whatman GF/F filters. Chl *a* in the 3 fractions was then extracted in 90 % acetone after Parsons et al. (1984) and measured with a Turner III scaling fluorometer. Nutrients (NO_3, NO_2, PO_4 and Si) were measured using a Technicon II AutoAnalyzer.

Phytoplankton production was measured using a photosynthetron (Lewis & Smith 1983) in which small volume (1 ml) short incubation time (40 min) ^{14}C incorporation was used to provide measurements of total

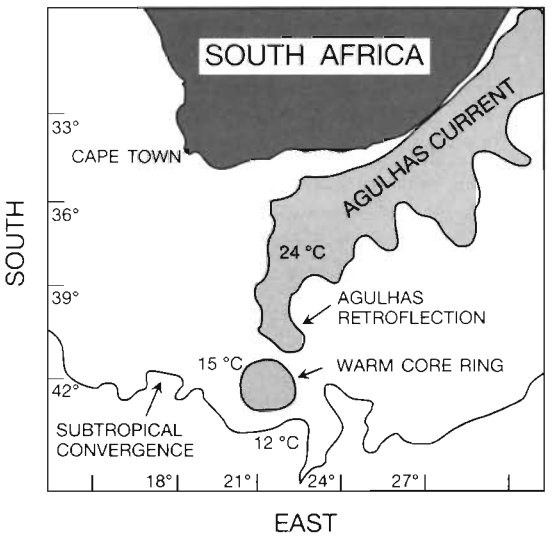

Fig. 1. Diagrammatic representation of a satellite image from 25 April 1991 showing the position of the warm-core ring shed from the Agulhas Retroflection and the Sub-Tropical Convergence

(dissolved and particulate) organic carbon fixation. Experimental procedures similar to those of Lewis & Smith (1983) were used. The specific activity of the ^{14}C was 608 µCi mg^{-1} and a concentration of 10 µCi ml^{-1} was used for each sample. A 2000 W tungsten-halogen lamp was used as a light source: photon flux (I) ranged from 0.33 to 1132.51 µE m^{-2} s^{-1}. Samples were counted in a Beckman liquid scintillation counter with efficiencies determined by the channels ratio method. Photosynthesis-Irradiance (P-I) models were fitted to the data using non-linear regression analysis to calculate the photosynthetic parameters, P^B_{max} and α^B. The model of Webb et al. (1974) fitted those plots not showing photoinhibition (symbol notations for Eqs. 1 to 10 are given in Table 1):

$$P^B = P^B_{max}\left[1 - \exp\left(\frac{-\alpha^B I}{P^B_{max}}\right)\right] \quad (1)$$

while that of Platt & Gallegos (1981) best fitted those showing photoinhibition:

$$P^B = f(I)\, g(I) \quad (2)$$

where

$$f(I) = P^B_s \tanh(I/I_s)] \quad (3)$$

$$g(I) = \frac{1}{2}\left[1 - \frac{I - I'_b}{[(I - I'_b)^m + I'^m_T]^{1/m}}\right] \quad (4)$$

Integrated production. To extrapolate from 2 point values of primary production, profiles of algal biomass

Table 1. Symbol notation and units for Eqs. 1 to 10 and other symbols used in text

Photosynthesis-irradiance parameters		
P^B	Production (normalised to biomass)	mg C (mg chl *a*)$^{-1}$ h^{-1}
P^B_{max}	Maximum production rate (photosynthetic capacity)	mg C (mg chl *a*)$^{-1}$ h^{-1}
$\int P$	Integrated production to 100 m	mg C (mg chl *a*)$^{-1}$ h^{-1} m^{-2} d^{-1}
α^B	Initial slope of P-I curve	mg C (mg chl *a*)$^{-1}$ h^{-1} (µE m^{-2} s^{-1})$^{-1}$
β	Slope of photoinhibition	mg C (mg chl *a*)$^{-1}$ h^{-1} (µE m^{-2} s^{-1})$^{-1}$
I	Irradiance	µE m^{-2} s^{-1}
I_b	Index of photoinhibition (P^B_s/β)	µE m^{-2} s^{-1}
I_k	Irradiance at saturation (light adaptation index)	µE m^{-2} s^{-1}
I_m	Irradiance optimal for photosynthesis	µE m^{-2} s^{-1}
I_z	Irradiance at depth z	µE m^{-2} s^{-1}
$I.$	Dimensionless (= I_z/I_k)	
Platt & Gallegos (1981) P-I model including inhibition		
P^B_s	Potential light saturated production rate	mg C (mg chl *a*)$^{-1}$ h^{-1}
I'_b	Irradiance at which $P^B = 0.5\ P^B_s$	µE m^{-2} s^{-1}
I_s	Theoretical saturating irradiance	µE m^{-2} s^{-1}
I_T	Threshold of photoinhibition	µE m^{-2} s^{-1}
I'_T	$I'_b - I_T$	µE m^{-2} s^{-1}
m	Geometrical scale factor (6) from Platt & Gallegos (1981)	
Gaussian curve parameters – nonuniform biomass profile		
B_z	Biomass at depth z	mg m^{-3}
B_0	Baseline chl *a* concentration	mg m^{-3}
h	Total biomass above baseline	mg m^{-2}
σ	Width of chlorophyll peak	m
z_m	Depth of chlorophyll maximum	m
Attenuation parameters		
K_z	Total attenuation coefficient	m^{-1}
K_w	Attenuation due to water	m^{-1}
K_c	Attenuation due to other substances	m^{-1}
Depth related parameters:		
z	Depth	m
z_{eu}	Depth of euphotic zone	m
z_{I_k}	Depth where irradiance = I_k	m
z_{mix}	Depth of mixed layer	m

and light are used to calculate integrated primary production. The assumption frequently made of a uniform biomass profile can lead to large errors, especially when establishing algorithms for interpreting satellite-derived data (Morel & Berthon 1989, Sathyendranath & Platt 1989). Many of the biomass profiles for this study showed sub-surface chlorophyll maxima. Consequently, a Gaussian curve was fitted to the data from which parameters were derived for the calculation of biomass at any depth z, so that

$$B_z = B_0 + \frac{h}{\sigma\sqrt{2\pi}} \exp\left[\frac{-(z - z_m)^2}{2\sigma^2}\right] \quad (5)$$

where B_0 = baseline pigment concentration (mg m^{-3}); σ = width of the chlorophyll peak (m); z_m = depth of the chlorophyll maximum (m); and h = total biomass above the baseline (mg m^{-2}).

The light profile is calculated as follows: Light at depth z is

$$I_z = I_{z-1} \exp(-K_z \Delta z) \quad (6)$$

where K_z = total attenuation coefficient and is itself a function of biomass and suspended particles:

$$K_z = K_w + (B_z\ K_c). \quad (7)$$

K_w (light attenuation due to water) and K_c (attenuation due to phytoplankton and other covarying substances) were not measured. Average K_z was measured and assumed to be K_z for the mixed layer depth. This was plotted against B_z calculated for the depth of the mixed layer for each station and then K_w and K_c were derived as the intercept and the slope respectively of this plot. Thus K_z for any depth z can be calculated.

Continuous measurements of photosynthetically available radiation (PAR) were not taken during the cruise. Consequently, to derive accurate estimates of water column production, daily irradiance was calculated according to Platt et al. (1990) on the basis of average insolation with 75 % cloud cover for the appropriate latitude. To reduce additional variation in the

data, all sampling days and all samples were treated in the same manner. Julian Day 112 was used (mid-date of the sampling period) as was latitude 42° S. During the cruise an average daily cloud cover of approximately 75% was recorded. Maximum noon photon flux under these conditions was thus calculated to be 745.5 μE m^{-2} s^{-1}.

P-I parameters (P^B_{max} and α^B) were only calculated at the surface and at 100 m for each station. The surface parameters were assumed to be constant throughout the mixed layer, where the mixed layer was less than 100 m outside the ring and at the ring edge. P^B_{max} and α^B were assumed to increase or decrease linearly between the mixed layer depth and 100 m. Inside the ring the mixed layer was always >100 m. A linear regression for P^B_{max} and α^B was calculated between the surface value and the 100 m value and used to generate P^B_{max} and α^B at any depth interval. Thus:

$$P_z = B_z P^B_{max} [1 - \exp(I_\bullet)] \quad (8)$$

where

$$I_\bullet = \frac{I_z}{I_k}, \quad (9)$$

$$I_k = \frac{P^B_{max}}{\alpha^B} \quad (10)$$

and therefore

$$\int P = \sum_{z=100}^{0} P_z. \quad (11)$$

For the 7 samples showing photoinhibition, the dimensionless parameter β/α^B was never >0.020. The effects of photoinhibition were therefore considered negligible and ignored with respect to daily water column production (see Platt et al. 1990).

RESULTS

Hydrography

The anti-cyclonic warm core ring, situated at 42° 11.8' S, 22° 13.7' E had a diameter of ±200 km and was characterised by the extension of the 10°C isotherm down to 750 m at its centre. Its maximum geostrophic velocity was 1 m s^{-1}. Temperature/salinity (θ/S) plots (Fig. 2) showed 2 separate water bodies; one characterised by warm saline water (Table 2) of virtually constant temperature and salinity to a depth of between 140 and 212 m and making up the main body of the ring. The other, surrounding the ring and including water from the STC towards the south, was

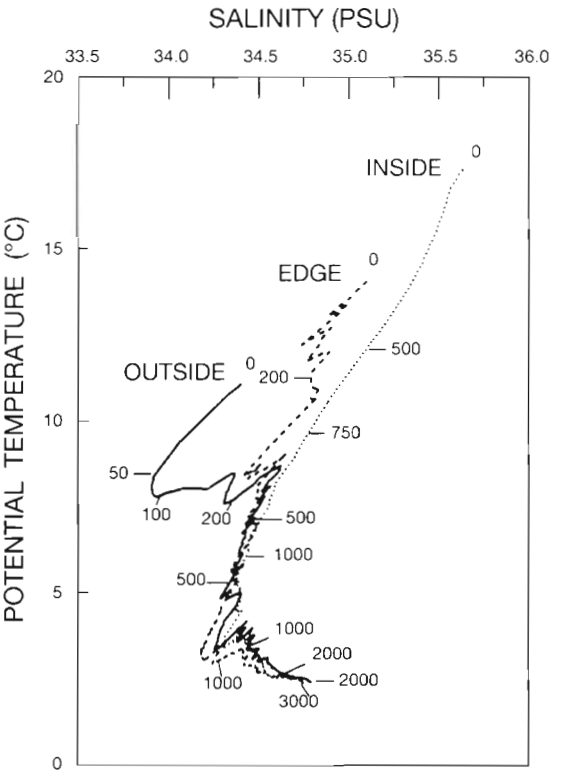

Fig. 2. Typical potential temperature (θ) vs salinity (S) plots of the inside, outside and edge of the ring. Numbers on the trace indicate depth (m)

colder, less saline and showed a reduced thermocline depth ranging from 12 to 80 m. At the confluence of these 2 water bodies, at the ring edge, salinities and temperatures were intermediate and more variable (Table 2). The distinction between the different water bodies was lost below about 750 m where the θ/S plots showed convergence at a potential temperature of ca 8°C. The 1% light depth ranged from 40 to 75 m outside the ring, 40 to 54 m at the edge of the ring and 38 to 92 m inside the ring. A more detailed description of the physical properties of the ring is given by Rigg (1991).

Table 2. Mean salinity and temperature data (± SE) for surface and deep samples at stations inside, outside and at the edge of the ring

Region	z (m)	Salinity (‰)	Temp. (°C)
Inside	0	35.615 ± 0.01	17.215 ± 0.08
	100	35.614 ± 0.01	17.225 ± 0.12
Edge	0	35.243 ± 0.12	15.133 ± 0.69
	100	34.933 ± 0.24	13.402 ± 1.24
Outside	0	34.694 ± 0.17	12.475 ± 1.10
	100	34.597 ± 0.09	10.918 ± 0.95

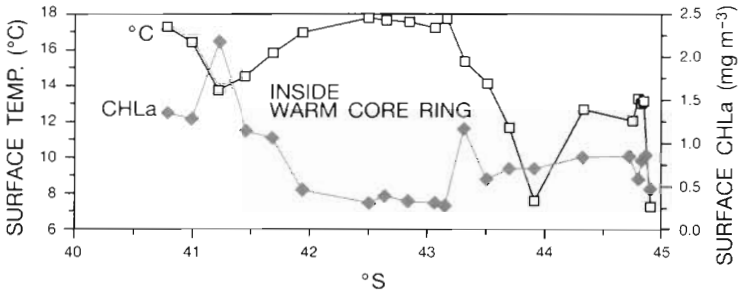

Fig. 3. Example of a north to south transect of surface temperature and chlorophyll *a* concentrations through the warm-core ring

Chlorophyll and primary production

An inverse relationship between surface temperature and surface chl *a* biomass was found (Fig. 3). Chl *a* concentrations decreased from ca 1.0 mg m^{-3} outside and at the ring edge to ca 0.4 mg m^{-3} in the warmer ring centre (Table 3). Size-fractionated surface chl *a* showed that about 56% of the phytoplankton were nano- and picoplanktonic (<20 µm) in the ring centre (Table 4). These smaller cells constituted only about one-third of the phytoplankton biomass outside the ring and at the ring edge. Depth-related differences in chl *a* concentration showed chl *a* outside the ring to decrease considerably from a mean of 1.09 ± 0.10 mg m^{-3} at the surface to 0.26 ± 0.06 at 100 m. At the edge, a decrease from 0.92 ± 0.07 mg m^{-3} at the surface to 0.41 ± 0.08 at 100 m was observed (Table 3). In some cases, chl *a* concentrations at 100 m were found to be 2 orders of magnitude lower than surface concentrations. In the centre of the ring, depth-related differences were negligible and average chl *a* concentrations at the surface and at 100 m were similar (0.43 ± 0.02 and 0.55 ± 0.11 mg m^{-3} respectively).

Surface nitrate concentrations averaged 1.54 ± 0.17 µmol l^{-1} in the centre, 2.54 ± 0.32 at the edge and 5.17 ± 1.00 outside the ring (Table 3). Nitrate concentrations outside and at the edge were roughly 3 µmol l^{-1} higher at 100 m than they were at the surface whereas inside the ring they were only about 0.1 µmol l^{-1} higher. Surface PO_4 concentrations averaged 0.20 ± 0.01 µmol l^{-1} in the ring centre, 0.29 ± 0.03 at its edge and 0.54 ± 0.09 in the surrounding water. Surface Si values for the corresponding regions averaged 2.95 ± 0.05, 2.17 ± 0.25 and 1.61 ± 0.09 µmol l^{-1} respectively. There was no significant change in these nutrient concentrations down to 100 m depth but by about 500 m depth, all nutrient concentrations had increased by at least an order of magnitude.

Considerable variability was found in the photosynthetic parameters (Table 5) leading to little distinction between the regions (Table 3). At the surface, the coefficient of variation (CV) ranged from 10 to 22% between regions for P^B_{max}, α^B and I_k while at 100 m, CV was between 15 and 25%. Within each region, CV ranged from over 100% for α^B at 100 m outside the ring to 20% for I_k at 100 m inside the ring. Because of the lack of clear regional distinctions in photosynthetic parameters we averaged P^B_{max}, α^B and I_k for all surface and 100 m stations. Mean P^B_{max} at the surface was 1.59 ± 0.13 mg C (mg chl *a*)$^{-1}$ h^{-1}, similar to that at 100 m (1.61 ± 0.29); mean α^B was 0.046 ± 0.01 mg C (mg chl *a*)$^{-1}$ h^{-1}(µE m^{-2} s^{-1})$^{-1}$ and 0.072 ± 0.02 at the surface and at 100 m respectively.

Depth-related differences in all 3 regions were highest for α^B and I_k while P^B_{max} inside the ring showed greater variability between surface and 100 m samples than either outside the ring or at the ring edge.

Photoinhibition occurred in 7 samples; 3 at the surface and 4 at 100 m (Table 6). Optimal photosynthetic light intensity or photoinhibition threshold, I_m, ranged from 93.3 to 182.0 µE m^{-2} s^{-1} for surface samples and typically 147.9 to 190.7 for deep samples, but only 36 for Stn 147. I_b, the index of photoinhibition, ranged from 1729 µE m^{-2} s^{-1} inside the ring to 5479 at the ring edge (Table 6).

Table 3. Mean (± SE) chlorophyll *a* (mg m^{-3}) and nitrate concentrations (µmol l^{-1}) and photosynthetic parameters P^B_{max} (mg C mg^{-1} chl *a* h^{-1}), α^B [mg C mg^{-1} chl *a* h^{-1} (µE m^{-2} s^{-1})$^{-1}$] and I_k (µE m^{-2} s^{-1}) for surface and deep samples at stations inside, outside and at the edge of the ring

Region	*z* (m)	Chl *a*	NO_3	P^B_{max}	α^B	I_k
Inside	0	0.431 ± 0.02	1.539 ± 0.17	1.44 ± 0.25	0.056 ± 0.01	35.0 ± 12.6
	100	0.550 ± 0.11	1.685 ± 0.18	1.88 ± 0.76	0.065 ± 0.03	29.1 ± 03.3
Edge	0	0.919 ± 0.07	2.542 ± 0.32	1.51 ± 0.17	0.055 ± 0.02	31.3 ± 05.5
	100	0.407 ± 0.08	5.150 ± 1.07	1.41 ± 0.35	0.093 ± 0.05	22.0 ± 07.3
Outside	0	1.091 ± 0.10	5.171 ± 1.00	1.75 ± 0.26	0.039 ± 0.01	47.6 ± 05.1
	100	0.256 ± 0.06	8.608 ± 1.10	1.61 ± 0.62	0.058 ± 0.03	34.4 ± 06.9

Table 4. Underway size-fractionated surface chlorophyll *a* concentrations (mg m^{-3}) for the 3 regions. Results are given as mean percentages ± SE

Region	Netplankton (<200, >20 µm)	Nanoplankton (<20, >3 µm)	Picoplankton (<3 µm)
Inside	40.94 ± 9.4	47.05 ± 9.4	9.37 ± 2.3
Edge	62.28 ± 6.3	20.05 ± 6.1	8.84 ± 1.2
Outside	61.16 ± 4.1	22.27 ± 3.8	8.28 ± 1.2

Integrated production

Calculations of integrated water column production to 100 m are presented in Table 5. Average hourly production ranged from 22.9 to 65 mg C m^{-2}. Mean integrated production was highest at the ring edge: 453 ± 56 mg C m^{-2} d^{-1} as opposed to 404 ± 78 and 287 ± 24 outside and inside the ring respectively. Although production inside the ring was between 30 and 35 % less than in the other 2 regions, in keeping with the 50 % lower chl *a* concentration found here, the statistical separation of the 3 regions is insignificant.

DISCUSSION

Hydrography

The hydrographic significance of warm core rings shed from the Agulhas Current Retroflection has become better understood recently. The entrainment of warm salty Indian Ocean water into the South Atlantic has a significant effect on the heat and freshwater budgets of the Atlantic Ocean, thereby affecting global climate through ocean-atmosphere heat and water fluxes. Indian Ocean water enters the South Atlantic at between 3 and 20 × 10^6 m^3 s^{-1}, driven pri-

Table 5. Production station data for the 3 regions showing latitude and longitude, chlorophyll *a* (mg m^{-3}) and nitrate concentrations (µmol l^{-1}), photosynthetic parameters (units as in Table 3) and integrated daily water column production, $\int P$ (mg C m^{-2} d^{-1}), for each. ND: not determined

Region Stn	*z* (m)	Latitude (S)	Longitude (E)	Chl *a*	NO_3	P^B_{max}	α^B	I_k	$\int P$
Inside									
117	0 100	42° 26.4'	23° 11.5'	0.291 0.396	2.013 1.885	ND 3.387	ND 0.117	ND 28.9	ND
157	0 100	42° 11.8'	22° 13.7'	0.375 0.375	1.720 1.665	1.039 0.920	0.063 0.039	16.5 23.6	240
161	0 100	42° 29.0'	22° 41.1'	0.500 0.375	2.140 1.865	1.383 ND	0.047 ND	29.4 ND	313
164	0 100	42° 28.1'	22° 42.3'	0.291 0.333	2.000 2.130	1.893 1.328	0.057 0.038	59.2 34.9	309
Edge									
137	0 100	41° 41.6'	22° 28.0'	0.583 0.907	1.685 2.580	1.370 0.441	0.082 0.032	16.7 13.8	421
147	0 100	41° 37.3'	21° 24.2'	0.916 0.208	3.350 15.125	1.992 1.366	0.069 0.225	28.9 6.1	610
151	0 100	41° 37.8'	21° 24.8'	1.041 0.416	3.280 7.807	1.471 1.876	0.038 0.051	38.7 36.9	437
172	0 100	43° 50.1'	24° 15.0'	1.124 0.583	2.260 3.383	1.220 1.936	0.031 0.062	40.7 31.2	345
Outside									
88	0 100	43° 55.1'	22° 31.1'	0.500 0.125	4.940 7.565	2.155 2.499	0.036 0.082	59.9 30.5	364
105	0 100	41° 08.8'	23° 20.1'	0.500 ND	1.200 ND	2.542 ND	0.066 ND	38.5 ND	686
127	0 100	43° 21.7'	21° 29.8'	0.874 0.192	8.613 17.820	1.580 2.841	0.048 0.124	32.9 22.9	436
177	0 100	44° 10.1'	24° 40.4'	0.999 0.694	10.343 11.285	1.224 0.470	0.022 0.010	55.6 47.0	279
181	0 100	44° 09.8'	24° 40.2'	0.749 0.827	10.920 12.063	1.232 0.630	0.024 0.017	51.3 37.3	254

Table 6. Photoinhibition parameters for the stations where inhibition was found (see Table 1 for notation and units)

Region Stn	z (m)	Photoinhibition parameters β	P^B_s	I_s	I_m	I_b
Inside						
157	0	2.6×10^{-4}	1.06	17.0	93	4115
164	100	7.7×10^{-4}	1.47	38.9	148	1729
Edge						
147	0	4.6×10^{-4}	2.07	30.1	151	4477
	100	7.4×10^{-4}	1.40	6.2	36	1889
151	0	4.7×10^{-4}	1.57	41.8	182	3319
	100	3.6×10^{-4}	1.96	38.7	191	5479
172	100	6.4×10^{-4}	2.05	32.9	152	3200

marily by ring and eddy shedding from the Agulhas Retroflection, a highly variable feature found between 22° and 13° E and following the northern boundary of the STC as it retroflects eastwards. Approximately 9 large anticyclonic rings are shed annually which move into the south, southeastern or northwestern South Atlantic. Some move in a southwesterly direction, cross the STC zone into colder South Atlantic water or turn back into the Indian Ocean (Lutjeharms & van Ballegooyen 1988, Walker & Mey 1988, Gordon & Haxby 1990, Wakker et al. 1990a, b, Duncombe Rae 1991, Gordon et al. 1992, Gründlingh 1992).

Persistent and cool westerly and southwesterly winds throughout the year cause rapid heat loss from the Agulhas Retroflection and associated rings. Water temperatures may decrease by ca 1.35 °C per month in the winter and by ca 0.25 °C per month in the summer. The closer the Retroflection or the rings are to the cold STC zone, the more rapidly they lose heat – as much as 200 W m^{-2}. In general, heat loss to the atmosphere is varied but even during the summer months it can exceed 100 W m^{-2} and in doing so changes the temperature, salinity and density structure of the surface mixed layer (Walker & Mey 1988, Gordon & Haxby 1990).

The ring examined during this study was characterised by warm saline water (ca 17.2 °C, 35.6 ‰) reminiscent of Agulhas Current water and indicative of a warm Agulhas Retroflection eddy. The deep mixed layer (>140 m) in the centre of the ring is maintained through convective overturning when colder surface water at the edges is drawn into the centre as heat is lost to the atmosphere. At the base of the ring the warmer water dissipates heat into the surrounding ocean. Outside the ring the low salinity water (ca 34.5 ‰) was characteristic of Sub-Antarctic Surface Water while the intermediate salinity (ca 35.0 ‰) at the edge of the ring arises from mixing processes across the boundary (Whitworth & Nowlin 1987). Water of decreasing salinity and temperature (from 8 to 3.5 °C) shown in the θ/S plot (Fig. 2) is indicative of Central SW Indian Ocean Water formed by subduction at the STC. Lowest salinity corresponded with water of 3.5 °C; a feature of Antarctic Intermediate Water, while increasing salinity at about 3000 m characterises North Atlantic Deep Water (Whitworth & Nowlin 1987).

The life span of such rings can be very varied. Some may last 2.5 yr (Gordon & Haxby 1990) while others may be undetectable to satellite thermal infrared imagery after 100 d although remaining visible to altimetry observations (Wakker et al. 1990b, Gründlingh 1992). Intermittent thermal infrared images indicated that this particular warm core ring had probably been in the same area for about 6 mo before we examined it. Afterwards, images showed that the ring was temporarily re-incorporated into a southerly filament of the Agulhas Retroflection (April) and released again towards the STC zone in August.

Phytoplankton biomass

Throughout the study region chl *a* concentrations ranged from 0.13 to 1.12 mg m^{-3} and are comparable to previous records for the same area (Plancke 1977, El Sayed et al. 1979, Allanson et al. 1981, Boden 1988, Perissinotto et al. 1992). Nevertheless, over scales of <50 km there were discrete differences in chlorophyll concentrations. In the ring centre, chlorophyll concentrations at 0 and 100 m averaged 0.43 and 0.56 mg m^{-3} respectively while at the edge values were 0.92 and 0.41 mg m^{-3} respectively and outside the ring they were 1.10 and 0.26 mg m^{-3} respectively.

An explanation for these observed differences requires a consideration of the light and nutrient environment as well as mixing depth, grazing pressure and community composition. Although nitrate concentrations were lowest inside the ring (1 to 2 µmol l^{-1}), this is not normally considered limiting, particularly for the nano- and picoplankton which dominated here (56 % by biomass) as they characteristically exhibit low V_{max} (maximum possible growth rate) and K_s (nutrient concentration at 0.5 V_{max}) values, allowing them to be competitive at low ambient nutrient concentrations and low rates of nitrogen regeneration (Furnas 1982, 1990, Probyn 1985, Probyn & Lucas 1987, Weber & El Sayed 1987). Similarly, PO_4 and Si concentrations were not considered to be limiting. Nevertheless, reduced Si concentrations outside the ring (1.61 ± 0.09 µmol l^{-1}) relative to within the ring (2.95 ± 0.05) may reflect the absence of diatoms in the nano- and picoplankton dominated community inside the ring. Furthermore, the observed P^B_{max} values for all regions and for both surface and deep communities showed no regional or

spatial differences, suggesting that the community was capable of photosynthesising maximally under favourable light conditions without evidence of nutrient stress.

A more likely explanation for the observed biomass differences is to be found in an examination of the mixing depth, the light environment and the photo-adaptiveness of the community (I_k).

For the STC latitude of 42° S and for 21 April (Julian Day 112), the light model of Platt et al. (1990) predicts that maximal noon PAR would be 745.5 μE m^{-2} s^{-1}. This translates into a value of 7.5 μE m^{-2} s^{-1} at a measured 1 % light depth of between 38 and 92 m within the ring where the average mixing depth was >140 m. I_k, the derived parameter signifying the onset of light saturation for the community within the ring ranges from 16 to 60 μE m^{-2} s^{-1}. The average I_k at 100 m (29 μE m^{-2} s^{-1}) is equivalent to the 26 % light depth or ± 15 m within the ring. Clearly then, the optimal photosynthetic depth is considerably shallower than the mixing depth of 140 m. While this type of analysis does not preclude photosynthesis at depths greater than that equivalent to I_k, this procedure does provide some measure of comparative analysis. We can do this in the form of ratios of mixing depth z_{mix}/1 % light depth (z_{eu}) and z_{I_k}/z_{mix} Larger values for the former and smaller values for the latter would point towards light limitation. A value of unity for z_{I_k}/z_{mix} would imply that the phytoplankton community could photosynthesise maximally over the entire mixing depth while values of <1.0 would imply that cells will experience light conditions unfavourable for maximum photosynthetic rates. Such an analysis for the 3 regions is given in Table 7.

Our analysis does indeed suggest that the light environment experienced by the phytoplankton community within the ring is least favourable while that outside the ring and particularly at the ring edge, is more favourable. It seems likely therefore that the low phytoplankton biomass recorded within the ring (0.43 ± 0.02 mg m^{-3}) is caused by deep convective mixing because of heat lost to the atmosphere which reduces water column stability, creating an unfavourable light environment. This was apparently particularly so for the netplankton community which dominated (62 %) in the better light and nutrient environment at the ring edge and outside the ring where the mixing depth was, on average, shallower than the euphotic depth (Table 7). The increased thermal stability and reduced mixing depth at the ring edge is clearly shown by the 10°C isotherm which demonstrates the warming influence of the ring on the surrounding cooler water (Rigg 1991).

Similar explanations for the control of phytoplankton biomass, size-structure, production and enhanced biomass in coastal waters and at oceanic fronts have been offered, among others, by Dugdale & Goering (1967), Pingree et al. (1976), Eppley & Peterson (1979), Denman & Gargett (1983), Holligan et al. (1984), Le Fèvre (1986) and McMurray et al. (1993). Our size-based biomass results agree with other studies in the Southern Ocean. Several studies in the Antarctic region (Hewes et al. 1990, Holm-Hansen & Mitchell 1991, Jacques & Panouse 1991) and in the Sub-Antarctic (El Sayed et al. 1979, Perissinotto et al. 1992) have shown that regions of high biomass such as frontal systems and the marginal ice-edge zone are generally dominated by netplankton while low biomass waters have an abundance of nano- and picoplankton. El Sayed et al. (1979) report a 70 to 100 % contribution by nanoplankton to the biomass of phytoplankton in the region of Crozet and Marion Islands (Southern Ocean). El Sayed (1988) notes that total integrated water column production averages about 66 % nanoplankton in Antarctic studies with picoplankton (<2 μm) often dominating the upper water column.

Table 7 Depth (m) where irradiance in the water column is equivalent to the I_k value (z_{I_k}), depth of mixed layer (z_{mix}) and depth of euphotic zone (z_{eu}) for all production stations. ND: not determined

Region Stn	z (m)	z_{I_k}	z_{mix}	z_{eu}	z_{I_k}/z_{mix}	z_{mix}/z_{eu}
Inside						
117	0	ND	153	38	ND	4.0
	100	27			0.2	
157	0	55	212	66	0.3	3.2
	100	50			0.2	
161	0	32	169	45	0.2	3.8
	100	ND			ND	
164	0	51	168	92	0.3	1.8
	100	61			0.4	
Edge						
137	0	37	35	45	1.1	0.8
	100	39			1.1	
147	0	28	25	40	1.1	0.6
	100	42			1.7	
151	0	26	36	40	0.7	0.9
	100	26			0.7	
172	0	34	31	54	1.1	0.6
	100	37			1.2	
Outside						
88	0	22	22	40	1.0	0.6
	100	28			1.3	
105	0	30	66	47	0.5	1.4
	100	43			0.7	
127	0	28	70	41	0.4	1.7
	100	31			0.4	
177	0	33	31	58	1.1	0.5
	100	35			1.1	
181	0	43	100	75	0.4	1.3
	100	49			0.5	

Grazing pressure by mesozooplankton and microzooplankton have undoubtedly also influenced the biomass and size-class spectrum although we have no data on this. It should also not be forgotten that the origin of the differing water masses may historically determine the community size-structure and biomass; particularly that of the warm-core ring whose water and entrained planktonic community probably originate from the subtropical region of the Madagascar channel.

Photosynthetic parameters and primary production

Despite temperature, salinity, nitrate and biomass differences between the inside of the ring and the surrounding water, there is considerable variability in the photosynthetic parameters, P^B_{max} and α^B and the derived parameter I_k, which obscures the relationship between photosynthesis and these bio-geochemical parameters. This is compounded by a lack of data on species composition.

As cells within the ring are likely to mix to 2 to 3 times as deep as the 1% light depth because of convective overturning, we might have expected to see shade-adapted P-I parameters. We found no evidence for this. On the other hand, at the ring edge the upper mixed layer (UML) was at least 10 m and at times over 20 m shallower than the 1% light depth. Here we could have expected surface populations to be adapted to higher light levels portrayed by low α^B and high I_k values. However, the opposite was found, with mean surface α^B and I_k being highest and lowest respectively. Certainly the deeper populations at 100 m and therefore below the UML should have exhibited dark adaptation as they would rarely have found themselves within the euphotic zone, nominally but not necessarily the 1% light depth. This is partially confirmed by the mean α^B at 100 m being high and I_k low although both showed marked variability. Outside the ring, surface I_k was on average higher, and α^B lower, indicating better adaptation to increased light levels consistent with an z_{mix}/z_{eu} value of near unity (Table 7) which implies that cells generally mixed entirely in the euphotic zone. However, we cannot explain the better apparent adaptation to light at stations (105 & 127) where mixing was below the euphotic zone.

Our results compare well with other studies at approximately the same latitude and elsewhere in the Antarctic area. For this region Allanson et al. (1981) recorded P^B_{max} between 0.44 and 1.12 mg C (mg chl *a*)$^{-1}$ m^{-3} while R. K. Laubscher's data (unpubl.) were more varied and P^B_{max} ranged from above 6 to below 0.4 mg C (mg chl *a*)$^{-1}$ m^{-3}. During the Antarctic summer Tilzer et al. (1985) found an average P^B_{max} of 0.687 ± 0.23 mg C (mg chl *a*)$^{-1}$ m^{-3}, average α^B of 0.0029 ± 0.0025 mg C (mg chl *a*)$^{-1}$ m^{-3}(μE m^{-2} s^{-1})$^{-1}$, and I_k ranging from 22 to 175 (μE m^{-2} s^{-1}) while during the winter Brightman & Smith (1989) recorded a mean surface P^B_{max} and α^B of 1.19 ± 0.6 mg C (mg chl *a*)$^{-1}$ m^{-3} and 0.021 ± 0.01 mg C (mg chl *a*)$^{-1}$ m^{-3}(μE m^{-2} s^{-1})$^{-1}$ respectively.

With deep and slow mixing there is the potential for surface and deep populations to exhibit photoadapted P-I parameters characteristic of high and low light intensities respectively. These expected differences between surface and deep phytoplankton populations were apparent in all 3 hydrographic areas. In all regions I_k was lower and α^B was higher for the deep samples indicating the anticipated enhanced adaptation to low light intensities with depth and indicative of a longer time spent in conditions of low light intensity. Differing regional phytoplankton taxonomic groups may also contribute to these effects. Harrison & Platt (1986) recorded higher α^B values with depth at similar latitudes in the northern hemisphere and Brightman & Smith (1989) found lower I_k values at 50 m than at the surface in Antarctic waters during the winter. Contrasting light regimes at the surface and at 100 m in all 3 regions are also likely to result in a differing depth related species composition. The maximum photosynthetic rate, P^B_{max}, was always lower at 100 m except inside the ring indicating some physiological differences caused by community effects. Harrison & Platt (1986) found that on a daily basis community structure was most important in accounting for depth-related differences in P^B_{max}. Species composition was not examined during this study but the dominance (56%) of nano- and picoplankton inside the ring and netplankton in the surrounding water (61%) suggests regional differences in population and or species structure. We can only speculate that this might account for trends in some of the photosynthetic parameters.

Despite uniform NO_3 concentration profiles we cannot exclude the likelihood that nitrogen re-supply rates in the deeper water exceed those in the surface, therefore enhancing primary production, although Harrison & Platt (1986) noted that neither phytoplankton biomass nor nitrate concentrations appeared important in explaining variations in photosynthetic parameters.

The onset of photoinhibition occurred at very low light levels (<200 μE m^{-2} s^{-1}), lower even than some winter Antarctic populations (Brightman & Smith 1989). Harrison & Platt (1986) found that a photoinhibition index, I_b, of 5000 W m^{-2} indicated that the photoinhibitory effects of light were minimal. We found that I_b ranged from 1729 to 5479 μE m^{-2} s^{-1} (ca 416 to ca 1320 W m^{-2}) which signifies relatively large inhibitory effects. That inhibition was not shown in all the samples may also indicate differences in species composition. However, the small number of samples showing inhibition precludes us

from drawing conclusions regarding susceptibility to inhibition or threshold irradiances.

Integrated production

Despite variable photosynthetic parameters within the 3 hydrographic regions, daily water column production integrated to 100 m was lowest inside the ring (287 ± 24 mg C m^{-2} d^{-1}), intermediate outside (404 ± 78) and highest at the ring edge (453 ± 56). Hourly production rates ranged from a minimum of 23 mg C m^{-2} h^{-1} inside the ring to a maximum of 66 outside the ring. This range is similar to other data from the Southern Ocean and the Antarctic (Allanson et al. 1981, Tilzer et al. 1985, Boden 1988). Depressed chl *a* concentrations inside the ring as well as deep mixing resulting in an unfavourable light environment contribute to the reduced production. On the other hand at the edge of the ring where elevated phytoplankton biomass and improved water column stability and light conditions were found, primary production was 35 % greater than in the ring centre and 5 % greater than outside the ring. Water column production was therefore closely related to the mixing depth and light regime as well as regional chl *a* concentrations. In this study, nutrient concentrations were probably not limiting. We can however conclude that production within the rings is about 30 % lower than the surrounding water with daily water column production in the area of the STC being 400 to 450 mg C m^{-2} d^{-1}.

The positive relationship between production and increasing phytoplankton biomass is in agreement with El Sayed et al. (1977), Plancke (1977), Allanson et al. (1981) and El Sayed (1988) for the same study area and for the Antarctic summer and winter months (Tilzer et al. 1985, Brightman & Smith 1989). Laws et al. (1990) report the same pattern for mid-latitudes in the northern hemisphere. Nevertheless, Table 8 shows that daily water column production can vary enormously, particularly in the Southern Ocean due mainly to extremes in algal biomass resulting from physical influences. In the open ocean biomass and productivity are lowest (Plancke 1977, Allanson et al. 1981, El Sayed 1988). Elevated chl *a* concentrations typify frontal zones such as the STC and the Antarctic Polar Front (Allanson 1981, Boden 1988) while maximum phytoplankton biomass and productivity have been recorded for the marginal ice-edge zone (Tilzer et al. 1985, Mitchell & Holm-Hansen 1991) and in particular the Sub-Antarctic islands (El Sayed 1988, Perissinotto et al. 1992). Water column stability created by ice melt may provide the necessary conditions for phytoplankton blooms during the Antarctic summer while the 'island mass effect' is responsible for greater and more persistent blooms surrounding the Sub-Antarctic islands (Table 8).

The physical processes causing elevated biomass at the ring edge are similar to those acting at most high-latitude oceanic fronts although on a smaller scale. At mid-latitude coastal shelf fronts such as the Ushant Front of the western English Channel, the horizontal mixing of

Table 8. Chlorophyll *a* and production data recorded during previous studies in the Southern Ocean

Source	Region	Chl *a* (mg m^{-3})	Production ([a, b, c])
Plancke (1977)	South of 40° S	0.32	0.34[a]
	Sub-Antarctic	0.17	0.17[a]
Allanson et al. (1981)	Southern Ocean 38–48° S (summer)	0.28–1.04	3–18[b]
	Southern Ocean 60–70° S (summer)	0.13–4.28	2–30[b]
Tilzer et al. (1985)	Antarctic (summer) (Bransfield Strait)	0.16–8.75	14.6–77.0[b]
Boden (1988)	Prince Edward Islands	2.3	175[b]
	Sub-Antarctic Ocean	0.2	10[b]
	Subtropical Front	1.7	88[b]
	Antarctic Polar Front	1.5	31[b]
El Sayed (1988)	Antarctic open ocean	<0.5	~100[c]
	Sub-Antarctic Islands	5–25	2800–3620[c]
Brightman & Smith (1989)	Antarctic (winter) (Bransfield Strait)	0.04–0.33	0.4–7.0[c]

[a]mg C m^{-3} h^{-1}; [b]mg C m^{-2} h^{-1}; [c]mg C m^{-2} d^{-1}

water introduces nutrients into oligotrophic surface waters to promote biological activity (Holligan et al. 1984, Le Fèvre 1986, Mann & Lazier 1991). The STC marks the boundary between warmer and generally nutrient depleted waters to the north and cooler nutrient rich waters of the Sub-Antarctic. Here, an intensification of thermal gradients and the horizontal mixing of nutrient rich waters by subduction is responsible for increased production at the northern boundary (Plancke 1977, Allanson et al. 1981, Lutjeharms et al. 1985). Elevated biomass at the Antarctic Polar Front has been attributed to upwelling and the stimulation of production based on regenerated nutrients and/or trace metal (e.g. Fe) availability (Allanson et al. 1981, de Baar et al. 1990) although we consider the light regime as a function of vertical mixing to provide a more likely control mechanism. Similarly, at ring or eddy margins deep nutrient rich water is brought to the surface during isopycnal mixing (Jeffrey & Hallegraeff 1987, Mann & Lazier 1991) which together with increased thermal stability can account for the increase in chl *a* concentrations and in primary production.

Synoptic estimates of primary production

Synoptic estimates of phytoplankton biomass and production are dependent upon ocean colour remote sensing and suitable algorithms developed from simultaneous measurements of photosynthetic parameters and optical properties in the water column. At this stage it is not possible to link 'ground truth' data to real time remote sensing but we can use past CZCS data to preliminarily define bio-optical or biogeochemical provinces for which there are reliable chlorophyll data.

Using information on the location of the STC (Lutjeharms & Valentine 1984) and calibrated CZCS data, a 7 yr (1979 to 1986) composite of chl *a* concentrations has been developed for the area between 15 and 48° E and 39 and 43° S (Weeks & Shillington unpubl.). This composit is divided into four 3-mo intervals representative of the 4 seasons. Surface chl *a* concentrations for the entire 7 yr period ranged from 0.15 to 2 mg m^{-3} (mean = 0.49) but showed no clear seasonal variation. Since most of our stations are within the boundaries of this 'province' and our surface chl *a* concentrations are similar to those found by Weeks & Shillington (unpubl.) we have used the same area to extrapolate our primary production data to this regional scale. Although Weeks & Shillington (unpubl.) found no clear seasonal variation in surface chlorophyll concentrations there is a 5-fold interannual variability in chlorophyll biomass. It is not known whether there are seasonal differences in sub-surface pigment concentrations or what effect the light regime has on primary production at different times of the year. Nevertheless we have extrapolated our estimates of integrated water column production in the designated area up to a full year for comparative purposes.

For a surface area of 1.264×10^6 km^2 and a daily production rate integrated to 100 m or 287 to 453 mg C m^{-2} d^{-1}, annual carbon fixation in our bio-optical province amounted to between 1.33×10^{-1} and 2.09×10^{-1} Gt C yr^{-1}. This amounts to approximately 0.5 to 0.8% of phytoplankton production in open ocean (3.1×10^8 km^2) and continental margin (5.9×10^7 km^2) seas combined (Walsh & Dieterle 1988). This confirms the importance of the STC in terms of production on a global scale as it is equivalent to an areal fixation rate of between 10.5×10^2 and 16.5×10^2 t C km^{-2} yr^{-1} which is intermediate between that of the world's open ocean and continental shelf regions where production is estimated at 6.0×10^2 and 20×10^2 t C km^{-2} yr^{-1} respectively (Walsh & Dieterle 1988). The STC south of Africa is therefore potentially a major sink for atmospheric CO_2.

While ocean colour remote sensing and P-I provide a useful tool for estimating basin-scale integrated total primary production, there remains the problem of distinguishing between new and regenerated production. It is the former that is available for export to consumers and/or to the benthos through sedimentation processes. To estimate CO_2 draw-down, measurements of 'new' production will be needed to augment P-I studies. Some interesting new developments in this are emerging, apart from *f*-ratio calculations, where the relationship between remotely sensed surface temperature, nitrate concentration and potential new production may yield a complementary approach to that of determining bio-optical provinces alone.

Acknowledgements. The authors gratefully acknowledge the financial support of the Department of Environment Affairs: South African National Antarctic Research Programme. We also thank the officers and crew of the MV 'SA Agulhas' as well as the ship-based scientists for their assistance during the cruise. We are indebted to Colin Attwood and Diane Gianakouras for analysing chl *a* and nutrient data. Roy van Ballegooyen is gratefully acknowledged for providing most of the physical oceanographic data and Scarla Weeks the remote sensing data. Trevor Platt and Shubha Sathyendranath provided invaluable assistance with the primary production calculations and together with John Field, commented constructively on the manuscipt at various stages. We thank the anonymous referees for their comments which improved the manuscript.

LITERATURE CITED

Allanson, B. R., Hart, R. C., Lutjeharms, J. R. E (1981). Observations on the nutrients, chlorophyll and primary production of the Southern Ocean south of Africa. S. Afr. J. antarct. Res. 10/11: 3–14

Boden, B. P. (1988). Observations of the island mass effect in the Prince Edward Archipelago. Polar Biol. 9: 61–68

Brightman, R. I., Smith, W. O. (1989). Photosynthesis-irradiance relationships of antarctic phytoplankton during austral winter. Mar. Ecol. Prog. Ser. 53: 143–151

de Baar, H. J. W., Buma, A. G. J., Nolting, R. F., Cadée, G. C., Jacques, G., Tréguer, P. J. (1990). On iron limitation of the Southern Ocean: experimental observations in the Weddell and Scotia Seas. Mar. Ecol. Prog. Ser. 65: 105–122

Denman, K. L., Gargett, A. E. (1983). Time and space scales of vertical mixing and advection of phytoplankton in the upper ocean. Limnol. Oceanogr. 28(5): 801–815

Dugdale, R. C., Goering, J. J. (1967). Uptake of new and regenerated forms of nitrogen in primary productivity. Limnol. Oceanogr. 12: 196–206

Duncombe Rae, C. M. (1991). Agulhas Retroflection rings in the south Atlantic Ocean: an overview. S. Afr. J. mar. Sci. 11: 327–344

El Sayed, S. Z. (1988). Productivity of the Southern Ocean: a closer look. Comp. Biochem. Physiol. 90B(3): 489–498

El Sayed, S. Z., Benon, P., David, P., Grindley, J. R., Murail, J.-F. (1979). Some aspects of the biology of the water column studied during the Marion-Dufresne cruise 08. C.N.F.R.A. (Com. Nat. fr. Rech. antarct.) 44: 127–134

Eppley, R. W., Peterson, B. J. (1979). Particulate organic matter flux and planktonic new production in the deep ocean. Nature 282: 677–680

Furnas, M. J. (1982). Growth rates of summer nanoplankton (<10 µm) populations in Lower Narragansett Bay, Rhode Island, USA. Mar. Biol. 70(1): 105–115

Furnas, M. J. (1990). In situ growth rates of marine phytoplankton : approaches to measurement, community and species growth rates. J. Plankton Res. 12: 1117–1151

Gordon, A. L. (1985). Indian-Atlantic transfer of thermocline water at the Agulhas retroflection. Science 227: 1030–1033

Gordon, A. L., Haxby, W. F. (1990). Agulhas eddies invade the south Atlantic: evidence from Geosat altimeter and shipboard conductivity-temperature-depth survey. J. geophys. Res. 95(C3): 3117–3125

Gordon, A. L., Weiss, R. F., Smethie, W. M., Warner, M. J. (1992). Thermocline and intermediate water communication between the south Atlantic and Indian Oceans. J. geophys. Res. 97(C5): 7223–7240

Gründlingh, M. L. (1992). Agulhas Current meanders: review and case study. S. Afr. Geogr. J. 74: 19–28

Harrison, W. G., Platt, T. (1986). Photosynthesis-irradiance relationships in polar and temperate phytoplankton populations. Polar Biol. 5: 153–164

Hewes, C. D., Sakshaug, E., Reid, F. M. H., Holm-Hansen, O. (1990). Microbial autotrophic and heterotrophic eucaryotes in Antarctic waters: relationships between biomass and chlorophyll, adenosine triphosphate and particulate organic carbon. Mar. Ecol. Prog. Ser. 63: 27–35

Holligan, P. M., Williams, P. J. leB., Purdie, D., Harris, R. P. (1984). Photosynthesis, respiration and nitrogen supply of plankton populations in stratified, frontal and tidally mixed shelf waters. Mar. Ecol. Prog. Ser. 17: 201–213

Holm-Hansen, O., Mitchell, B. G. (1991). Spatial and temporal distribution of phytoplankton and primary production in the western Bransfield Strait region. Deep Sea Res. 38: 961–980

Jacques, G., Panouse, M. (1991). Biomass and composition of size fractionated phytoplankton in the Weddell-Scotia Confluence area. Polar Biol. 11: 315–328

Jeffrey, S. W., Hallegraeff, G. M. (1987). Phytoplankton pigments, species and light climate in a complex warm-core eddy of the East Australian Current. Deep Sea Res. 34(5/6): 649–673

Kuring, N., Lewis, M. R., Platt, T., O'Reilly, J. E. (1990). Satellite derived estimates of primary production on the northwest Atlantic continental shelf Cont. Shelf Res. 10(5): 461–484

Laws, E A., DiTullio, G. R., Carder, K. L., Betzer, P. R., Hawes, S. (1990). Primary production in the deep blue sea. Deep Sea Res. 37(5): 715–730

Le Fèvre, J. (1986). Aspects of the biology of frontal systems. In: Blaxter, J. H., Southward, A. J. (eds.) Advances in marine biology 23. Academic Press, London, p. 164–301

Lewis, M. R., Smith, J. C. (1983). A small volume, short-incubation-time method for measurement of photosynthesis as a function of incident irradiance. Mar. Ecol. Prog. Ser. 13: 99–102

Lutjeharms, J. R. E. (1989). The role of mesoscale turbulence in the Agulhas Current system. In: Nihoul, J. C. J., Jamart, B. M. (eds.) Mesoscale/Synoptic coherent structures in geophysical turbulence. Elsevier Science Publishers B.V., Amsterdam, p. 357–372

Lutjeharms, J. R. E , Valentine, H. R. (1984). Southern Ocean thermal fronts south of Africa. Deep Sea Res. 31(12): 1461–1475

Lutjeharms, J. R. E. , van Ballegooyen, R. C. (1988). The retroflection of the Agulhas Current. J. phys. Oceanogr. 18(11): 1570–1583

Lutjeharms, J. R. E. , Valentine, H. R. (1988). Evidence for persistent Agulhas rings south-west of Cape Town. S. Afr. J. Sci. 84: 781–783

Lutjeharms, J. R. E. , Walters, N. M., Allanson, B. R. (1985). Oceanic frontal systems and biological enhancement. In: Siegfried, W. R., Condy, P. R., Laws, R. M. (eds.). Antarctic nutrient cycles and food webs. Springer-Verlag, Berlin, p. 11–21

Mann, K. H., Lazier, J. R. N. (1991). Dynamics of marine ecosystems. Blackwell Scientific Publications, Oxford

McMurray, H. F., Carter, R. A., Lucas, M. I. (1993). Size-fractionated phytoplankton production in western Agulhas Bank continental shelf waters. Cont. Shelf Res. 13(2/3): 307–329

Mitchell, B. G., Holm-Hansen, O. (1991). Observations and modeling of the Antarctic phytoplankton crop in relation to mixing depth. Deep Sea Res. 38: 981–1007

Morel, A., Berthon, J.-F. (1989). Surface pigments, algal biomass profiles, and potential production of the euphotic layer: relationships reinvestigated in view of remote-sensing applications. Limnol. Oceanogr. 34(8): 1545–1562

Mueller, J. L., Lange, R. E. (1989). Bio-optical provinces of the Northeast Pacific Ocean: a provisional analysis. Limnol. Oceanogr. 34(8): 1572–1586

Parsons, T. R., Maita, Y., Lalli, C. M. (1984). A manual of chemical and biological methods for seawater analysis. Pergamon Press, Oxford

Perissinotto, R., Laubscher, R. K., McQuaid, C. D. (1992). Marine productivity enhancement around Bouvet and the South Sandwich Islands (Southern Ocean). Mar. Ecol. Prog. Ser. 88: 41–53

Pingree, R. D., Holligan, G. T., Mardell, G. T., Head, R. N. (1976). The influence of physical stability on spring, summer and autumn phytoplankton blooms in the Celtic Sea. J. mar. biol. Ass. U. K. 56: 845–873

Plancke, J. (1977). Phytoplankton biomass and productivity in the Subtropical Convergence area and shelves of the western Indian subantarctic Islands. In: Llano, G. A. (ed.) Adaptations within Antarctic ecosystems; proceedings of the third SCAR symposium on Antarctic biology. Gulf Publishing Co., Houston, p. 51–73

Platt, T., Gallegos, C. L. (1981). Modelling primary production. In: Falkowski, P. (ed.) Primary productivity in the sea. Plenum Press, New York, p. 339–362

Platt, T., Sathyendranath, S., Caverhill, C. M., Lewis, M. R. (1988). Ocean primary production and available light: further algorithms for remote sensing. Deep Sea Res. 35(6): 855–879

Platt, T., Sathyendranath, S., Ravindran, P. (1990). Primary production by phytoplankton: analytic solutions for daily rates per unit area of water surface. Proc. R. Soc. Lond. B 241: 101–111

Probyn, T. A. (1985). Nitrogen uptake by size-fractionated phytoplankton populations in the southern Benguela upwelling system. Mar. Ecol. Prog. Ser. 22(3): 249–258

Probyn, T A., Lucas, M. I. (1987). Ammonium and phosphorous flux through the microplankton community in Agulhas Bank waters. In: Payne, A. I. L., Gulland, J. A., Brink, K. H. (eds.) The Benguela and comparable ecosystems. S. Afr. J. mar. Sci. 5: 209–222

Rigg, G. (1991). Correspondence between the surface and subsurface expression of some mesoscale oceanic features in South African water. Honours thesis, University of Cape Town

Sathyendranath, S., Platt, T. (1989). Remote sensing of ocean chlorophyll: consequence of non-uniform pigment profile. Appl. Opt. 28: 490–495

Sathyendranath, S., Platt, T., Caverhill, C. M., Warnock, R. E , Lewis, M. R. (1989). Remote sensing of oceanic primary production: computations using a spectral model. Deep Sea Res. 36(3): 431–453

Tilzer, M. M., von Bodungen, B., Smetacek, V. (1985). Light-dependence of phytoplankton photosynthesis in the Antarctic Ocean: implications for regulating productivity. In: Condy, P. R., Laws, R. M. (eds.) Antarctic nutrient cycles and food webs. Springer-Verlag, Berlin, p. 60–69

Wakker, K. F., Naeije, M. C., Scharroo, R., Ambrosius, B. A. C. (1990a). Extraction of mesoscale ocean currents information from Geosat altimeter data. In: Proc. of the Space and Sea Colloquium, E.S.A. S.P.-312. European Space Agency, Paris, p. 221–226

Wakker, K. F., Zandbergen, R. C. A., Naeije, M. C., Ambrosius, B. A. C. (1990b). Geosat altimeter data analysis for the oceans around South Africa. J. geophys. Res. 95(C3): 2991–3006

Walker, N. D., Mey, R. D. (1988). Ocean/atmosphere heat fluxes within the Agulhas Retroflection region. J. geophys. Res. 93(C12): 15472–15483

Walsh, J. J., Dieterle, D. A. (1988). Use of satellite ocean colour observations to refine understanding of global geochemical cycles. In: Rosswall, T., Woodmansee, R. G., Risser, P. G. (eds.) Scales and global change. Wiley, New York, p. 287–317

Webb, W. L., Newton, M., Starr, D. (1974). Carbon dioxide exchange of *Alnus rubra*. A mathematical model. Oecologia 17: 283–293

Weber, L. H., El Sayed, S. Z. (1987). Contributions of the net, nano- and picoplankton to the phytoplankton standing crop and primary productivity in the Southern Ocean. J. Plankton Res. 9: 973–994

Whitworth, T., Nowlin, W. D. (1987). Water masses and currents of the Southern Ocean at the Greenwich Meridian. J. geophys. Res. 92(C6): 6462–6476

This article was submitted to the editor

Manuscript first received: September 24, 1992
Revised version accepted: February 12, 1993